Three Dimensional Carbon Nanotube Scaffolds for Long-Term Maintenance and Expansion of Human Mesenchymal Stem Cells

Article *in* Journal of Biomedical Materials Research Part A · March 2017

DOI: 10.1002/jbm.a.36062

6 authors, including:

Gaurav Lalwani
Stony Brook University
26 PUBLICATIONS **533** CITATIONS
SEE PROFILE

Sunny C Patel
Stony Brook University
14 PUBLICATIONS **81** CITATIONS
SEE PROFILE

Yahfi Talukdar
Stony Brook University
8 PUBLICATIONS **102** CITATIONS
SEE PROFILE

Balaji Sitharaman
Stony Brook University
125 PUBLICATIONS **3,927** CITATIONS
SEE PROFILE

Society For Biomaterials

Three-dimensional carbon nanotube scaffolds for long-term maintenance and expansion of human mesenchymal stem cells

Gaurav Lalwani, Michael D'agati, Anu Gopalan, Sunny C. Patel, Yahfi Talukdar, Balaji Sitharaman

Department of Biomedical Engineering, Stony Brook University, Stony Brook, New York 11794-5281

Received 28 December 2016; revised 2 March 2017; accepted 7 March 2017
Published online 00 Month 2017 in Wiley Online Library (wileyonlinelibrary.com). DOI: 10.1002/jbm.a.36062

Abstract: Expansion of mesenchymal stem cells (MSCs) and maintenance of their self-renewal capacity *in vitro* requires specialized robust cell culture systems. Conventional approaches using animal-derived or artificial matrices and a cocktail of growth factors have limitations such as consistency, scalability, pathogenicity, and loss of MSC phenotype. Herein, we report the use of all-carbon 3-D single- and multiwalled carbon nanotube scaffolds (SWCNTs and MWCNTs) as artificial matrices for long-term maintenance and expansion of human MSCs. Three-dimensional SWCNT and MWCNT scaffolds were fabricated using a novel radical initiated thermal cross-linking method that covalently cross-links CNTs to form 3-D macroporous all-carbon architectures. Adipose-derived human MSCs showed good cell viability, attachment, proliferation, and infiltration in MWCNT and SWCNT scaffolds comparable to poly(lactic-co-glycolic) acid (PLGA) scaffolds (baseline control). ADSCs retained stem cell phenotype after 30 days and satisfied the International Society for Cellular Therapy's (ISCT) minimal criteria for MSCs. Post expansion, (1) ADSCs showed *in vitro* adherence to tissue culture polystyrene (TCPS); (2) MSC surface antigen expression [CD14(−), CD19(−), CD34(−), CD45(−), CD73(+), CD90(+), CD105(+)]; and (3) trilineage differentiation into osteoblasts, adipocytes, and chondrocytes. Results show that cross-linked 3-D MWCNTs and SWCNTs scaffolds are suitable for *ex vivo* expansion and maintenance of MSCs for therapeutic applications. © 2017 Wiley Periodicals, Inc. J Biomed Mater Res Part A: 00A:000–000, 2017.

Key Words: mesenchymal stem cells, carbon nanotubes, three-dimensional, scaffolds, expansion, maintenance

How to cite this article: Lalwani G, D'agati M, Gopalan A, Patel SC, Talukdar Y, Sitharaman B. 2017. Three-dimensional carbon nanotube scaffolds for long-term maintenance and expansion of human mesenchymal stem cells. J Biomed Mater Res Part A 2017:00A:000–000.

INTRODUCTION

Mesenchymal stem cells (MSCs) are multipotent nonhematopoietic stem cells capable of direct multilineage differentiation into mesodermal cell lineages such as osteoblasts, adipocytes, chondrocytes, and connective stromal cells and transdifferentiation into ectodermal and endodermal cell types such as neurons and muscle cells.[1] MSCs show promise for several therapeutic applications including regenerative medicine, drug discovery, cellular therapy, and disease modeling.

Conventional approaches for expansion of stem cells and maintenance of their self-renewal capacity employ *in vitro* 2-D systems consisting of tissue culture polystyrene flasks and dishes along with animal derived or artificial matrices and a cocktail of growth factors. These 2-D systems have several limitations such as consistency, scalability, and pathogenicity (risk of infection).[2] Additionally, MSCs, upon expansion during prolonged culture on 2-D tissue culture substrates, undergo significant changes in phenotype such as diminished proliferation potential, senescence or loss of "stemness," and genomic alterations.[3–5]

Three-dimensional culture systems have been recommended to overcome the limitations of 2-D systems.[3,6,7] Three-dimensional cell cultures allow high cell densities and maintain a greater pool of stem cells. Furthermore, 3-D culture systems provide a better understanding of cellular mechanisms that guide stem cell behavior.[8] Several approaches utilizing 3-D culture systems for stem cell expansion *in vitro* have been developed. These approaches can be classified into 3 categories: (1) MSCs cultured as cell aggregates.[9,10] Expansion of MSCs as 3-D aggregates is usually associated with spontaneous differentiation and demands efficient downstream approaches to purify cultures into a desired cell type.[11] (2) MSCs expanded in 3-D gel-based microcapsules[12] and microcarriers.[13,14] MSCs encapsulated in 3-D porous microcarrier beads are protected from shear stresses, although diffusion of oxygen and nutrients within beads can be limited. Furthermore, one challenge associated with microcarrier culture is optimization of cell-harvesting protocols to guarantee efficient cell-bead separation and high cell recovery without compromising viability or functionality.[15,16] (3) MSCs

Additional Supporting Information may be found in the online version of this article.
Correspondence to: B. Sitharaman, Ph.D.; Department of Biomedical Engineering, Bioengineering Building, Room 115, Stony Brook University, Stony Brook, NY 11794-5281, USA; e-mail: balaji.sitharaman@stonybrook.edu
Contract grant sponsor: National Institute of Health; contract grant number: 1DP2OD007394-01

cultured on 3-D matrices fabricated using polymers,[8,17] ceramic materials,[18,19] or decellularized matrices.[3,20] Limitations associated with 3-D porous scaffolds are hypoxia and inefficient retrieval or recovery of cells after long-term expansion.[21,22] Although enzymatic (e.g., using trypsin) dissociation approaches are efficient for recovery of cells in the scaffold's periphery, it is difficult to isolate cells from the central regions of the scaffolds due to low enzymatic penetration as a result of limited passive diffusion.

Carbon nanomaterials can be divided into 3 classes: (1) zero-dimensional fullerenes, (2) one-dimensional carbon nanotubes (CNTs), and (3) two-dimensional graphene, all of which have been used for several biomedical applications.[23–31] CNTs are one-dimensional tubular nanofibers. They are broadly classified as single-walled (SWCNTs), double-walled (DWCNTs), and multiwalled CNTs (MWCNTs). These CNTs have been deposited using CVD and vacuum filtration on 2-D glass substrates for stem cell maintenance and differentiation.[32–37] Holy et al. have reported enhanced cell adhesion and maintenance of pluripotent stem cells in an undifferentiated state on MWCNT-coated glass substrates.[34] Brunner et al. have reported that altering the surface roughness of MWCNT films can influence adhesion, proliferation, and colony morphology of human embryonic stem cells and envision the development of MWCNT-coated films as tunable surfaces for the control of stem cell behavior.[33] Mooney et al. have reported the differentiation of MSCs into osteoblasts, adipocytes, and chondrocytes on COOH-functionalized MWCNT substrates.[37] Recently, Pryzhkova et al. showed differentiation of human pluripotent stem cells into all three embryonic germ layers that can be controlled by the nanotopography and surface roughness of CNT arrays.[36] Although these studies are promising, to harness the remarkable physiochemical properties of CNTs for stem cell expansion and maintenance, it is critical to achieve assembly into 3-D architectures. Recent 3-D all-CNT assemblies (fabricated using CVD or sacrificial template-transfer methods) have been reported to be cytocompatible substrates.[38,39] However, the ability of fabrication methods to control the porosity of 3-D CNT scaffolds or form covalent bonds between CNTs (important for mechanical stability of scaffolds for *in vivo* biomedical applications) still needs to be demonstrated. Additionally, none of these 3-D substrates to date has been reported to facilitate stem cell maintenance and expansion.

We have employed radical initiated thermal cross-linking and annealing of CNTs to fabricate chemically cross-linked 3-D macro-sized (>1 cm in all 3 dimensions), free-standing, all-carbon scaffolds. This method can fabricate macroporous (20 nm–300 μm pore sizes) 3-D all-carbon structures with high porosities (~80–85%). The porosity of scaffolds can be controlled by the amount of radical initiator used in the cross-linking process, thereby allowing the fabrication of porous all-carbon scaffolds tailored toward specific applications. This novel fabrication method is economical, facile, and scalable, and shows potential to overcome limitations of the above fabrication methods.[40–42]

In this study, we report the capability of these 3-D CNT scaffolds to support MSC maintenance and expansion. We investigated (1) the cell viability, attachment and proliferation of human adipose-derived stem cells (ADSCs) on SWCNT and MWCNT scaffolds and (2) the plasticity or "stemness" of ADSCs after long-term culture on 3-D SWCNT and MWCNT scaffolds according to the International Society for Cellular Therapy (ISCT) guidelines.[43] ADSCs post-long-term expansion on 3-D SWCNT or MWCNT scaffolds were harvested and examined *in vitro* for (a) adherence to plastic (TCPS), (b) MSC surface antigen expression [CD14(−), CD19(−), CD34(−), CD45(−), CD73(+), CD90(+), CD105(+)], and (c) *in vitro* trilineage differentiation into osteoblasts, adipocytes, and chondrocytes. Porous 3-D polymeric scaffolds prepared using the FDA-approved biodegradable biocompatible polymer poly(lactic-co-glycolic acid) (PLGA) were used as controls.

MATERIALS AND METHODS

Fabrication and characterization of MWCNT, SWCNT, and PLGA scaffolds

MWCNTs (Sigma–Aldrich, NY, USA), SWCNTs (CheapTubes Inc., NY, USA), PLGA (Polysciences Inc., PA, USA), benzoyl peroxide (BP, Sigma–Aldrich, NY, USA), and chloroform ($CHCl_3$, Fisher Scientific, PA, USA) were used as purchased. Porous PLGA scaffolds with ~85% porosity were fabricated using a thermal cross-linking particulate leaching technique using NaCl as the porogen as described previously.[44] MWCNT and SWCNT scaffolds were fabricated by mixing nanomaterials with BP at a mass ratio of MWCNT/SWCNT:BP = 1:0.05 as described previously.[40] Detailed protocols on the characterization of scaffolds using scanning electron microscopy (SEM), micro-computed tomography (micro-CT), Brunauer–Emmett–Teller (BET) surface area and pore size distribution, and SEM image processing are included in the Supporting Information.

Cell culture

Human ADSCs were purchased from Lonza Walkersville Corp. (MD, USA). ADSCs were grown in Lonza's ADSC human Adipose Derived Stem Cell Growth BulletKit™ Medium containing 10 vol % fetal bovine serum (FBS, Gibco Life Technologies, NY, USA) and 1 vol % antibiotics (penicillin–streptomycin, Gibco Life Technologies, NY, USA). Media was changed twice a week, and cells were maintained at 37°C in a humidified environment of 5% CO_2–95% O_2. For cytocompatibility studies, purified MWCNT and SWCNT scaffolds were prepared as described in the Supporting Information.

Lactate dehydrogenase (LDH) assay

Lactate dehydrogenase was performed to assess the membrane integrity of ADSCs cultured on PLGA, MWCNT, and SWCNT scaffolds. Briefly, after each time point (1, 3, and 5 days), 50 μL media was collected from each well of the 24-well plate ($n = 6$ for each scaffold group) and transferred to a fresh 96-well plate. A total of 100 μL of LDH assay mixture was added to each well and incubated in dark for 45

min. To stop the reaction, 1 *N* HCl (10% volume) was added to each well. Absorbance values were recorded using a 96-well-plate reader (Molecular Devices, CA, USA) at 490 nm. Positive control cells (100% dead) were prepared by incubating ADSCs grown on tissue culture polystyrene with lysis buffer for 45 min before centrifugation. Cells cultured on PLGA scaffolds served as the baseline control. Total LDH release (% of positive control) was expressed as the percentage of $(OD_{test} - OD_{blank})/(OD_{positive} - OD_{blank})$, where OD_{test} is the optical density of cells cultured on PLGA, MWCNT, or SWCNT scaffolds; OD_{blank} is the optical density of 96-well plate without cells; and $OD_{positive}$ is the optical density of positive control (100% dead cells). Absorbance of blank culture media was measured for baseline correction.

Calcein-AM fluorescence imaging

Calcein-AM imaging was performed to stain live cells on PLGA, MWCNT, and SWCNT scaffolds. Calcein-AM dye is internalized by living cells and converted to green fluorescent calcein upon hydrolysis by intracellular esterases. Therefore, calcein-AM is used to selectively stain live, metabolically active cells. Briefly, after 1, 3, 5, 15, and 30 days of ADSC culture on PLGA, MWCNT, and SWCNT scaffolds, media was removed and scaffolds were washed with PBS. One milliliter of Calcein-AM dye (4 μ*M*) was added to each well and incubated at 37°C in dark for 20 min. The scaffolds were transferred to 35-mm glass-bottom dishes (Mattek Corporation, Ashland, MA) and imaged by a confocal laser-scanning microscope (Zeiss LSM 510 Meta NLO Two-Photon) using Zeiss LSM Image Browser software (version 4.2, Carl Zeiss Microimaging, Thornwood, NJ).

Immunofluorescence for focal adhesion and cell proliferation

Immunofluorescence was performed to visualize focal adhesion complex protein vinculin and cell proliferation marker Ki-67. Briefly, glutaraldehyde fixed cells on PLGA, MWCNT, and SWCNT scaffolds were washed with PBS and incubated with 2% glycine for 5 min for blocking. The scaffolds were placed in 0.5% Triton-X-100 permeabilizing buffer (composition: 10.3 g sucrose, 0.4 g Hepes buffer, 0.06 g $MgCl_2$, 0.29 g NaCl, and 0.5 mL Triton-X-100 in 100 mL of DI water) for 25 min. Scaffolds were then washed with immunofluorescence buffer (IFB, 0.1% Triton-X-100 and 0.1% BSA in PBS) and incubated with commercially available monoclonal antibodies. Scaffolds were incubated for 1 h with either antiproliferating Ki-67 antibody (2 μL/mL in IFB, Cat. No. P8825, Sigma Aldrich, New York, USA) for cell proliferation analysis or monoclonal anti-vinculin antibody (2 μL/mL in IFB, Cat. No. V4139, Sigma Aldrich, NY, USA) for visualization of focal adhesion sites. After 1 h of incubation with primary antibodies, the scaffolds were washed with IFB (3×) and incubated with secondary antibody (anti-rabbit TRITC, 2 μL/mL in IFB, Cat. No. T6778, Sigma Aldrich, New York, USA) for 1 h. Scaffolds were then washed with IFB (3×) and the cytoplasm was stained with FITC-conjugated phalloidin (2 μL/mL in PBS) for 1 h to visualize actin filaments (cytoskeleton). Samples were imaged using a confocal laser-scanning microscope (Zeiss LSM 510 Meta NLO Two-Photon) equipped with Zeiss LSM Image Browser software (version 4.2, Carl Zeiss Microimaging, Thornwood, NJ).

SEM imaging for cell attachment

To visualize cell attachment on scaffolds, glutaraldehyde-fixed cells on PLGA, MWCNT, and SWCNT scaffolds were subjected to dehydration steps using graded ethanol washes (70%–100%), air dried, and vacuum dried for 24 h. Scaffolds were then sputter coated with 3 nm of silver (Ag) and imaged using a JOEL 7600 F Analytical high-resolution SEM (Center for Functional Nanomaterials, Brookhaven National Laboratory, New York) at an accelerating voltage of 2 kV.

Image processing to assess cellular infiltration

Z-stacks of calcein-stained ADSCs on PLGA, MWCNT, and SWCNT scaffolds were acquired using a confocal laser-scanning microscope (Zeiss LSM 510 Meta NLO Two-Photon). Individual Z-stacks were then imported to ImageJ (Bethesda, MD, USA) and subjected to spectral coding using a time-lapse color coder plugin to false-color each slice as a function of depth (Z height, i.e., depth of cellular infiltration). The multiple spectrally color-coded slices of Z-stacks were then compressed to form one composite image and reported.

Analysis of MSC phenotype (ISCT guideline)

MSCs express specific surface antigens that can be used as markers for identification of stem cell phenotype in a heterogeneous population of cells. According to ISCT guidelines, MSCs are CD14(−), CD19(−), CD34(−), CD45(−), CD73(+), CD90(+), and CD105(+).[43] Immunofluorescence was performed on ADSCs attached to PLGA, MWCNT, or SWCNT scaffolds after 15 days of culture using the protocol described in the section "Immunofluorescence for focal adhesion and cell proliferation" with a few modifications. We used FITC-conjugated monoclonal antibodies specific to each surface antigen to assess the expression of MSC markers on ADSC cultured on PLGA, MWCNT, and SWCNT scaffolds after 15 days. The cytoplasm was stained using Rhodamine phalloidin to visualize actin filaments (red fluorescence, Life Technologies, USA).

Adherence of MSCs to tissue culture polystyrene (ISCT guideline)

According to ISCT guidelines, stem cells must be adherent to plastic when maintained in standard tissue culture conditions.[43] After 30 days of culture on PLGA, MWCNT, and SWCNT scaffolds, ADSCs were harvested from the scaffolds and expanded *in vitro* on 150 mm TCPS plates. The cells were cultured in ADSC basal growth media using standard tissue culture protocols as described in the section "Cell culture".

Multilineage differentiation of expanded MSCs (ISCT guidelines[43])

Osteogenic differentiation. ADSCs harvested from PLGA, SWCNT, and MWCNT scaffolds after 30 days of culture were used for differentiation studies. Additionally ADSCs grown

on TCPS (not PLGA, SWCNT, or MWCNT scaffolds) were used as controls. Osteogenic differentiation was performed using manufacturers protocol (Lonza Corporation MD, USA). Osteogenic induction media was prepared by mixing hMSC differentiation basal medium—osteogenic and SingleQuots™ factors (dexamethasone, L-glutamine, ascorbate, Pen/Strep, and MCGS) as supplied in the hMSC Osteogenic BulletKit (Catalog # PT 3002, Lonza Corp., MD, USA). Initially, ADSCs were plated at a density of 10,000 cells per well in a 24-well plate and incubated in ADSC basal growth media for 24 h at 37°C, 5% CO_2, and 90% humidity. After 24 h, growth media was removed and 1 mL of osteogenic induction media was added to each well and replenished every 3–4 days. ADSCs were maintained in osteogenic induction media for 3 weeks. Alkaline phosphatase expression and alizarin red staining were used as markers for osteogenic differentiation (detailed protocols are included in the Supporting Information).

Adipogenic differentiation. Adipogenic differentiation was performed using a well-established procedure reported previously.[45] Briefly, mixing hMSC adipogenic induction medium (PT-3102B) and the following SingleQuots™ prepared adipogenic induction medium: h-insulin (recombinant), L-glutamine, MCGS, dexamethasone, indomethacin, IBMX (3-isobutylmethyl xanthine), and GA-1000. Adipogenic maintenance medium was prepared by mixing hMSC adipogenic maintenance medium (PT-3102 A) and the following SingleQuots™: h-insulin (recombinant), L-glutamine, MCGS, and GA-1000. All components were purchased as hMSC Adipogenic BulletKit (Catalog number PT-3004, Lonza Corporation, MD, USA). ADSCs were plated at a cell density of 20,000 cells per milliliter in 24-well plates and incubated in ADSC basal growth media for 24 h at 37°C, 5% CO_2, and 90% humidity. After incubation, ADSCs were subjected to three cycles of adipogenic induction/maintenance wherein each cycle consisted of culturing ADSCs in adipogenic induction media for 3 days and adipogenic maintenance media for 3 days. After 3 cycles, ADSCs were maintained in adipogenic maintenance media for an additional 7 days. The cells were rinsed with PBS (3×), fixed using 4% paraformaldehyde for 20 min, and stained using Oil red O dye for characterization of triglycerides and esters as a marker for adipogenic differentiation (detailed protocol included in the Supporting Information).

Chondrogenic differentiation. Chondrogenic differentiation was performed according to the manufacturers protocol (Lonza Corporation MD, USA). Briefly, incomplete chondrogenic induction medium was prepared by mixing hMSC differentiation basal medium—chondrogenic and the following SingleQuots™: dexamethasone, ascorbate, ITS + supplement, GA-1000, sodium pyruvate, proline, and L-glutamine. Complete chondrogenic media was prepared by adding TGF-β to incomplete chondrogenic media to achieve a final concentration of 10 ng/mL. ADSC were trypsinized and centrifuged (5000 rpm, 5 min) to obtain a cell pellet. The cell pellet was washed with incomplete chondrogenic media, centrifuged, and resuspended in complete chondrogenic media. An aliquot of 2.5×10^5 cells were added to a 15 mL sterile poly(propylene) culture tubes with 1 mL complete chondrogenic media and centrifuged at 5000 rpm for 5 min to obtain a cell pellet. Caution was maintained not to disrupt the pellet throughout the differentiation study. The caps of the tubes were loosened by one half turn to facilitate gas exchange and the tubes were incubated at 37°C, 5% CO2, and 90% humidity for 28 days with regular media changes every 2–3 days. After 28 days, the pellets were harvested, fixed with formalin, and embedded in paraffin for histological sectioning. Alcian blue staining was performed to assess chondrogenic differentiation (detailed protocol included in Supporting Information).

Statistical analysis

Data are reported as mean ± standard deviation. Statistical analysis was performed for a 95% confidence interval ($p < 0.05$) using students "t" test. To analyze the differences between the groups, one-way ANOVA followed by Tukey Kramer *post hoc* analysis was performed.

RESULTS

Fabrication of PLGA, MWCNT, and SWCNT scaffolds

PLGA scaffolds were fabricated using a thermal cross-linking particulate leaching method using NaCl as a porogen.[44] Three-dimensional MWCNT and SWCNT scaffolds were fabricated using a radical initiated thermal cross-linking method using MWCNT and SWCNT as building blocks.[40] Figure 1(A) displays the digital images of PLGA, MWCNT, and SWCNT scaffolds used for cell culture studies. The scaffolds were macroscopic cylinders of ~4 mm in height and 3–4 mm in diameter. Figure 1(B) shows the images of SWCNT scaffolds assembled in various sizes to illustrate the scalability of fabrication method.

Characterization of PLGA, MWCNT, and SWCNT scaffolds

Scanning electron microscopy. Figure 1(C) displays the representative SEM images of PLGA, MWCNT, and SWCNT scaffolds. PLGA scaffolds show characteristic cubic shaped pores with pore sizes between 250 and 500 μm (size of NaCl crystals). MWCNT and SWCNT scaffolds show interconnected nanoscale cross-links forming a 3-D architecture. The nanotube mesh appears porous with irregularly shaped pores.

Microcomputed tomography. MicroCT has been extensively used to determine the porosity and pore sizes of 3-D polymeric and all-carbon scaffolds. Figure 1(D) displays the representative 3-D microCT reconstructions of PLGA, MWCNT, and SWCNT scaffolds. The porosity values of PLGA, MWCNT, and SWCNT scaffolds determined by microCT reconstructions were 85.0 ± 2.4%, 89.6 ± 2.0%, and 83.1 ± 5.7%, respectively. The macropore diameter for PLGA, MWCNT, and SWCNT scaffolds were between 250 and 500 μm, 100 and 400 μm, and 150 and 550 μm, respectively. The CNT scaffolds possess nanoscale pores that are not visualized by microCT [white solid interconnect structures in Fig. 1(D)] due to a resolution limit of 6 μm. These pores are visualized

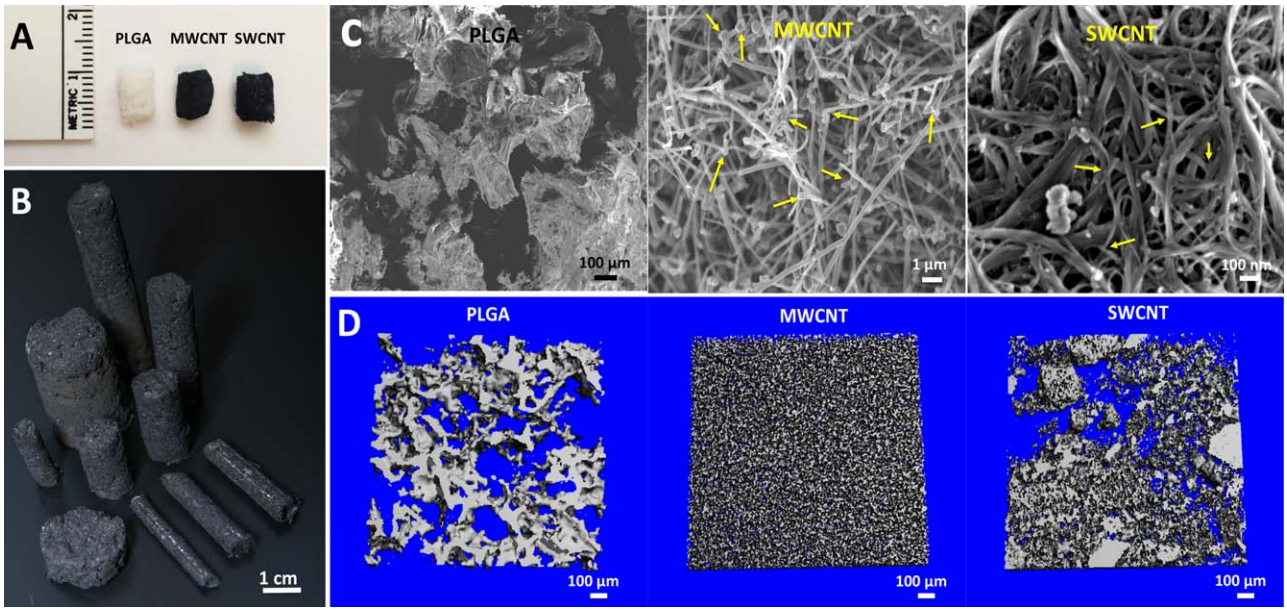

FIGURE 1. A: Optical images of representative 3-D PLGA, MWCNT, and SWCNT scaffolds. Cylindrical scaffolds of 6–9 mm height and 4–5 mm diameter were used for cell culture experiments. B: SWCNT scaffolds assembled in various sizes to illustrate the scalability of fabrication method (scale bar is 1 cm). C: Representative scanning electron microscopy images of PLGA, MWCNT, and SWCNT scaffolds. Arrows correspond to the formation of nanoscale cross-links between carbon nanotubes. D: Representative 3-D microCT reconstructions of PLGA, MWCNT, and SWCNT scaffolds. Void spaces (porosity) inside scaffolds are represented by blue color.

by SEM imaging [Fig. 1(C)] and can be quantified using SEM image processing and BET analysis.

BET surface area analysis. BET adsorption using nitrogen gas was used to determine the surface area and pore sizes of MWCNT and SWCNT scaffolds using single point measurements. The BET surface area of MWCNT and SWCNT scaffolds was 50.62 and 91.74 m^2/g, respectively (Table I). The average pore diameter of MWCNT and SWCNT scaffolds was 250 and 750 Å, respectively.

Image processing for porosity analysis. SEM image processing has been extensively used to characterize the porosity and pore diameter of 3-D tissue engineering scaffolds. Nanoscale porosities are important for efficient transport of nutrients and waste metabolites inside a 3-D scaffold. To quantify the nanoscale porosities of MWCNT and SWCNT scaffolds, SEM images were subjected to a series of image processing steps. The porosity and pore sizes of PLGA scaffolds were accurately determined using microCT and they lack the presence of nanoporosities. Therefore, SEM image processing was used only for MWCNT and SWCNT scaffolds. The porosity values of MWCNT and SWCNT scaffolds were $48.35 \pm 4.25\%$ and $37.98 \pm 2.95\%$, respectively. The nanopore diameter of MWCNT and SWCNT scaffolds was 20–900 nm and 15–950 nm, respectively (Table I).

Image processing for surface roughness analysis. Nanotopography of tissue engineering scaffolds plays a significant role in influencing cellular behavior by altering cell attachment, proliferation, and gene and protein expression. ImageJ was used to determine the nanoscale roughness of 3-D MWCNT and SWCNT scaffolds. SEM images (8 bit) with pixel intensity values between 0 a.u. and 255 a.u. (black–white) were used for this analysis. Therefore, the calculated roughness values are not in absolute units and are suitable only for a qualitative comparison between MWCNT and SWCNT scaffolds. The mean surface roughness (R_q) values for MWCNT and SWCNT scaffolds were 129.2 ± 15.65 a.u. and 90.41 ± 18.07 a.u., respectively. The arithmetic surface roughness (R_a) values of MWCNT and SWCNT scaffolds were 137.9 ± 13.39 a.u. and 109.51 ± 16.6 a.u., respectively. The MWCNT scaffolds showed a greater surface roughness than SWCNT scaffolds (Table I).

Lactate dehydrogenase (LDH) assay

Lactate dehydrogenase is a cytosolic enzyme released in the culture media by apoptotic or necrotic cells. LDH assay quantifies the amount of LDH released as a measure of cell death. The LDH present in the culture media catalyzes the conversion of lactate to pyruvate, in turn reducing NAD+ to NADH, which catalyzes the conversion of iodonitrotetrazolium present in the assay reagent (INT) to a water-soluble formazan product that can be quantified using an absorbance plate reader. Figure 2(A) shows the total LDH released (normalized to positive controls) from ADSCs after 1, 3, and 5 days of culture on PLGA, MWCNT, and SWCNT scaffolds. Although ADSCs on SWCNT scaffolds show a slightly higher LDH release (~45%) compared to cells grown on TCPS (~33%) after day 1, no significant differences were observed between total LDH released by ADSCs cells on PLGA, MWCNT, and SWCNT scaffolds at all time points (LDH release was between ~30 and 45% for all groups).

TABLE I. Porosity, pore sizes and surface roughness of scaffolds.

	Porosity		Pore Sizes				Surface Roughness	
Scaffolds	MicroCT (%)	SEM Image Processing (%)	MicroCT (μm)	SEM Image Processing (nm)	BET (N_2 Gas, Å)	Surface Area (BET)	Mean (R_q, a.u.)	Arithmetic (R_a, a.u.)
PLGA	84.97 ± 2.36	-	250–500	-	-	-	-	-
MWCNT	89.55 ± 1.98	48.35 ± 4.25	100–400	20–900	250	50.62	129.20 ± 15.65	137.90 ± 13.39
SWCNT	83.14 ± 5.69	37.98 ± 2.95	150–550	15–950	750	91.74	90.41 ± 18.07	109.51 ± 16.60

Calcein-AM fluorescence imaging

Calcein-AM is a nonfluorescent dye, which upon cellular internalization, is converted to green fluorescent calcein due to removal of acetoxymethyl ester group by intracellular esterases, and is retained in the cytoplasm of living cells. Therefore, it is widely used to stain living eukaryotic cells.[27] Figure 2(B) shows the representative calcein-AM-stained images of ADSCs cultured on PLGA [Fig. 2(1–5)], MWCNT [Fig. 2(6–10)], and SWCNT [Fig. 2(11–15)] scaffolds after 1, 3, 5, 15, and 30 days. Presence of live ADSCs was observed after 24 h of culture on PLGA, MWCNT, and SWCNT scaffolds as observed in Figure 2(1, 6, and 11), respectively. For each scaffold group, an increase in the number of green-fluorescent cells was observed from D1 to D30. ADSCs on all scaffold groups on D30 appear to be confluent and uniformly distributed.

Immunofluorescence for focal adhesion and cell proliferation

Cell attachment: focal adhesion (vinculin). Vinculin is a membrane cytoskeletal protein important for the formation of focal adhesion assembly and has been widely used as a marker to characterize cell–matrix adhesion.[46] Figure 3 shows the representative images of ADSCs cultured on PLGA [Fig. 3(A–C)], MWCNT [Fig. 3(D–F)], and SWCNT [Fig. 3(G–I)] scaffolds. ADSCs are stained green using FITC-phalloidin for cytoskeleton (green fluorescence) and fluorescently labeled antibodies for vinculin expression (red fluorescence). To ascertain co-localization of red and green fluorescence and corroborate the absence of nonspecific signal, merged images are also presented. Figure 3(B,E,H) confirms the expression of vinculin by ADSCs cultured on PLGA, MWCNT, and SWCNT scaffolds, respectively. The vinculin protein appears to be co-localized with actin filaments [Fig. 3(A,D,G)] and evenly distributed throughout the cytoplasm [Fig. 3(C,F,I)].

Cell proliferation: ki-67 expression. Ki-67 is an antigen expressed during the active phases of cell cycle (G1, S, G2, and mitosis). The expression of Ki-67 is absent during the G0 phase; therefore, it has been widely used as a marker of cell proliferation.[47] Figure 3 shows the representative confocal microscopy images of immunofluorescence staining for Ki-67 expression by ADSCs cultured on PLGA [Fig. 3(J–L)], MWCNT [Fig. 3(M–O)], and SWCNT [Fig. 3(P–R)] scaffolds after 5 days. ADSCs were stained with FITC conjugated phalloidin for actin cytoskeleton [green fluorescence, Fig. 3(J,M,P)] and fluorescently labeled antibodies for Ki-67 expression (red fluorescence, Fig. 3(K,N,Q)]. Figure 3(L,O,R) shows the merged images for actin cytoskeleton and Ki-67 protein. Ki-67 expression can be observed throughout the cytoplasm and nucleus for cells seeded on PLGA [Fig. 3(K,L)], MWCNT [Fig. 3(N,O)], and SWCNT [Fig. 3(Q,R)] scaffolds suggesting that ADSCs on all scaffold groups were metabolically active and proliferating.

SEM imaging for cell attachment

SEM was used for the characterization of cellular adhesion and morphology. Figure 4 shows the representative SEM images of ADSCs on PLGA [Fig. 4(A)], MWCNT [Fig. 4(B)], and SWCNT [Fig. 4(C)] scaffolds after 5 days. The cells appear horizontally spread out on all scaffold groups (white arrows, Fig. 4). ADSCs on all the scaffolds show formation of cytoplasmic extensions and membrane projections with no preferential direction. Figure 4(D,E) is a representative high-magnification SEM image of ADSCs on MWCNT scaffolds. Formation of filopodia that attach and wrap around the underlying nanotube network can be clearly visualized [yellow arrows, Fig. 4(D,E)].

Image processing to assess cellular infiltration

Cellular infiltration inside PLGA, MWCNT, and SWCNT scaffolds was assessed by image processing of Z-stacks of calcein-AM-stained ADSCs. Each individual stack was subjected to spectral-color coding steps to false color cells as a function of Z depth, that is, cellular infiltration. Figure 4(F–H) shows the infiltration of cells on PLGA, MWCNT, and SWCNT scaffolds, respectively. Presence of cells can be detected upto a depth of ~200–450 μm for each scaffold group. Image acquisition beyond that depth was not possible due to limitations with laser penetration inside 3-D scaffolds.

Immunofluorescence for MSC phenotype analysis

Surface antigens have been extensively used for the identification of specific cell populations. According to ISCT guidelines, MSCs should express CD73, CD90, and CD105, whereas lack the expression of hematopoietic cell markers such as CD14, CD19, CD34, and CD45.[43] Figure 5 shows the representative immunofluorescence images of ADSCs stained for various stem cell markers after 15 days of culture on PLGA [Fig. 5(a)], MWCNT [Fig. 5(b)], and SWCNT [Fig. 5(c)] scaffolds. Cells were stained with rhodamine phalloidin (red fluorescence) for actin cytoskeleton and

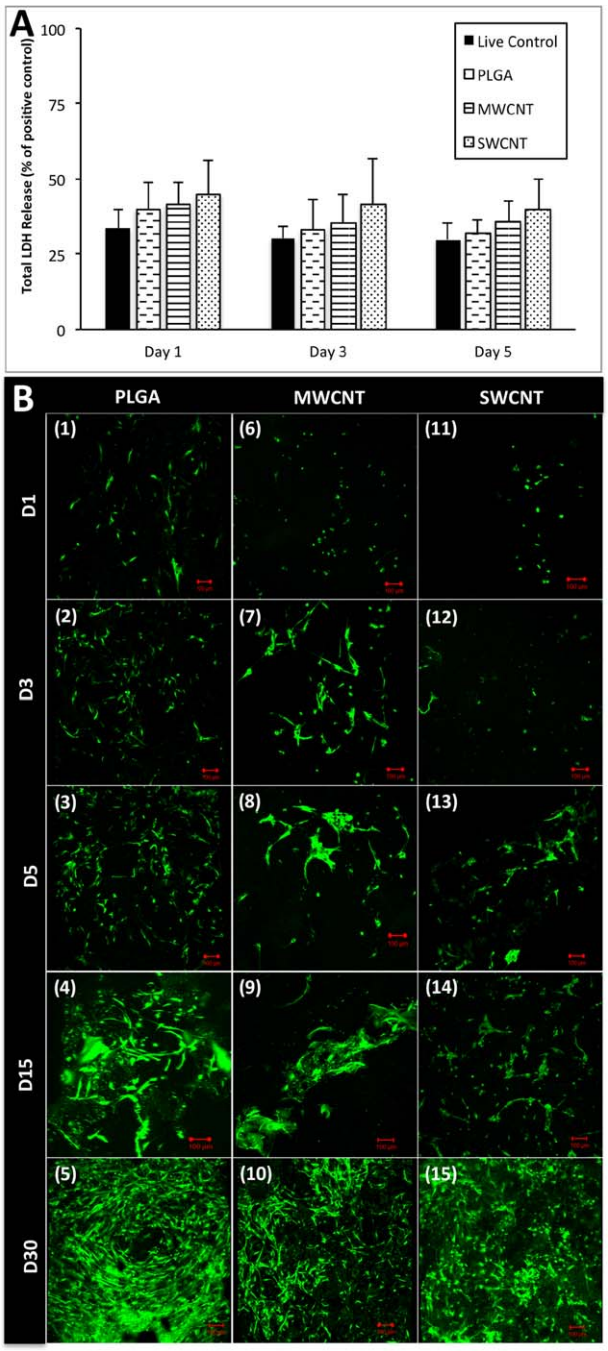

FIGURE 2. A: Cytotoxicity evaluation using lactate dehydrogenase assay after 1, 3, and 5 days of ADSC culture on TCPS (live control) and 3-D PLGA, MWCNT, and SWCNT scaffolds. Chart represents total LDH release (%) normalized to positive controls (100% dead cells). Data are represented as means ± standard deviation. B: Representative calcein-AM-stained green fluorescence images of ADSCs on 3-D PLGA (1–5), MWCNT (6–10), and SWCNT scaffolds (11–15) after 1, 3, 5, 15, and 30 days of culture. Presence of live ADSCs on the scaffolds can be observed. Scale bars are 100 μm.

FITC-conjugated monoclonal antibodies (green fluorescence) for MSC surface antigens. ADSCs on all scaffold groups express CD73, CD90, and CD105, whereas lack the expression of CD14, CD19, CD34, and CD45, thereby satisfying the criteria for MSC phenotype.

Multilineage differentiation of expanded MSCs (ISCT guidelines)

Osteogenic differentiation. Alkaline phosphatase (ALP) activity. Alkaline phosphatase is an early-stage osteogenic marker.[48] Figure 6(A) shows the ALP activity of ADSCs trypsinized and expanded *in vitro* after 30 days of culture on PLGA, MWCNT, and SWCNT scaffolds. ALP activity between the groups ranged from ∼1.8 to 3 μ*M*/ng dsDNA with ADSCs isolated from SWCNT scaffolds showing a significant decrease in ALP expression compared to control ADSCs cultured on TCPS. ADSCs isolated from PLGA and MWCNT scaffolds showed a similar level of ALP activity as control ADSCs.

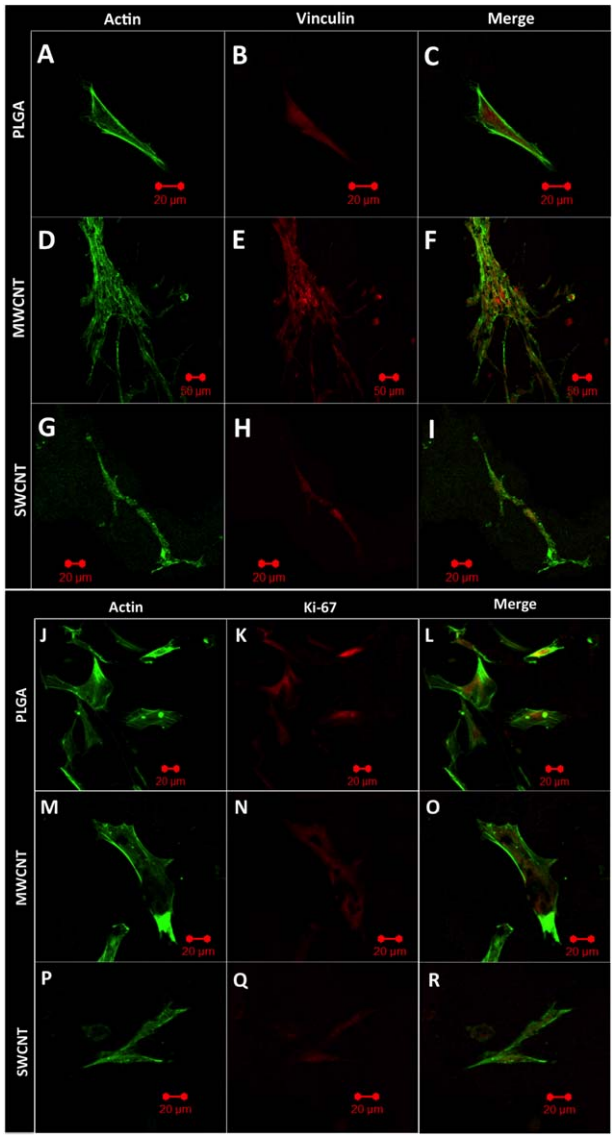

FIGURE 3. Representative immunofluorescence images of ADSCs cultured on PLGA (A–C and J–L), MWCNT (D–F and M–O), and SWCNT (G–I and P–R) scaffolds after 5 days of culture. ADSCs are stained green for actin (cytoskeleton) and red (mAb for vinculin–focal adhesion marker (A–I) and Ki-67-cell proliferation marker (J–R)). Merged images are shown to confirm co-localization of cytoplasm and focal adhesion and cell proliferation markers.

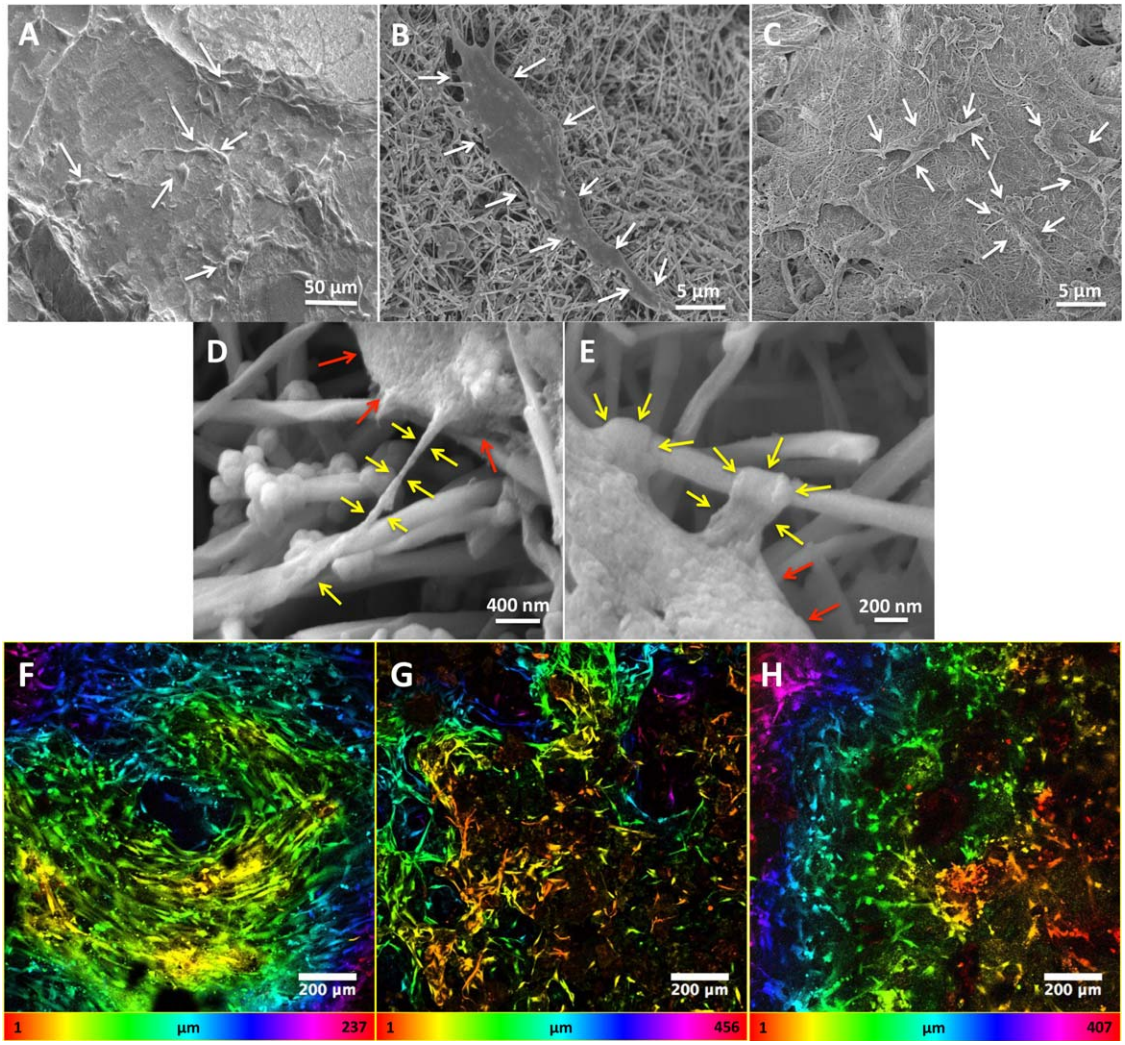

FIGURE 4. Representative SEM images showing adhesion of ADSC on (A) PLGA, (B) MWCNT, and (C) SWCNT scaffolds. Formation of cytoplasmic extensions (filopodia and pseudopodia) can be observed for all scaffold groups. Images (D) and (E) are high-magnification images of ADSCs on MWCNT scaffolds. ADSCs extend numerous cytoplasmic extensions (yellow arrows) that wrap around and attach to the underlying nanotube mesh. Red arrows correspond to cell body. (F–H) Representative spectrally color-coded images of calcein-AM-stained ADSCs as a function of confocal *Z*-depth (i.e., cellular infiltration) after 5 days of culture on (F) PLGA, (G) MWCNT, and (H) SWCNT scaffolds. Presence of cells can only be detected upto a depth of ~200–450 μm for MWCNT and SWCNT scaffolds and ~240 μm for PLGA scaffolds due to limitations associated with laser penetration depth.

Alizarin red staining. Alizarin red binds to calcium deposits in the extracellular matrix (ECM) and has been widely used to detect the presence of calcium in ECM of osteogenic cells.[45] ADSCs isolated from PLGA [Fig. 6(C)], MWCNT [Fig. 6(D)], and SWCNT [Fig. 6(E)] scaffolds after 30 days of culture show good deposition of calcium in the ECM (red staining, black arrows), comparable to control ADSCs [Fig. 6(B)]. There was no difference in distribution of the staining pattern between various scaffold groups compared to control ADSCs.

Adipogenic differentiation. Oil red O staining. Oil red O is a fat-soluble dye that specifically stains triglycerides, cholesteryl esters, and neutral lipids without staining biological membranes.[49] ADSCs isolated from PLGA, MWCNT, and SWCNT scaffolds [Fig. 6(G–I)] show the presence of intracellular fat vacuoles (red stain, black arrows) similar to ADSCs cultured on TCPS controls [Fig. 6(F)]. The fat vacuoles appear to be distributed throughout the cytoplasm.

Chondrogenic differentiation. Alcian blue staining. Alcian blue is widely used to stain acidic polysaccharides such as glycosaminoglycans (GAGs) present in the extracellular matrix of chondrocytes.[50] Figure 6(A–D) show the representative Alcian blue-stained images of ADSCs cultured on TCPS (control) and ADSCs isolated from PLGA, MWCNT, and SWCNT scaffolds, respectively, after chondrogenic differentiation. The blue color shows the deposition of GAGs in the ECM. No significant differences were observed between all experimental groups.

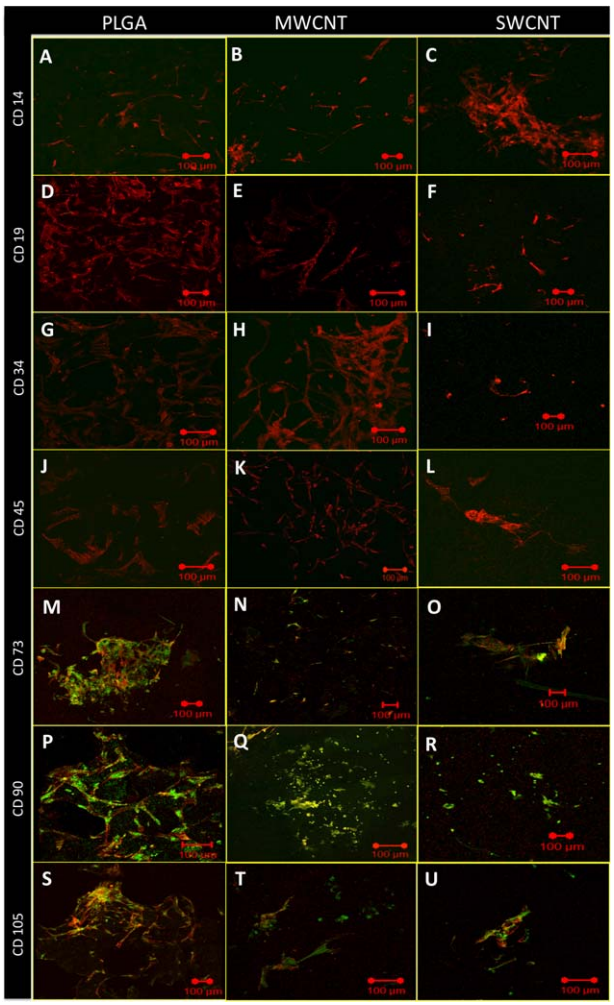

FIGURE 5. Representative immunofluorescence images of ADSCs showing the presence/absence of MSC surface antigens (A–C) CD14, (D–F) CD19, (G–I) CD34, (J–L) CD45, (M–O) CD73, (P–R) CD90, and (S–U) CD105 after 15 days of culture on PLGA, MWCNT, and SWCNT scaffolds. ADSC are stained with rhodamine phalloidin (red fluorescence) for cytoplasm and FITC-conjugated mAbs against MSC antigens (green fluorescence). Green fluorescence is absent in images (A–L) and co-localized with red fluorescence in images (M–U).

DISCUSSIONS

The overall objective of this study was to investigate the suitability of 3-D macro-sized chemically cross-linked porous CNTs scaffolds as synthetic matrices for human stem cell expansion and maintenance. Optical images of 3-D MWCNT, SWCNT, and PLGA scaffolds are shown in Figure 1(A). We have previously reported the use of BP as a radical initiator to induce thermal cross-linking of CNTs and graphene toward the fabrication of 3-D all-carbon architectures.[40,51] BP decomposes into benzoyl and benzoyloxyl free radicals that attack the C=C sp^2 bonds on CNT structure forming active centers that serve as inter nanotube cross-linking sites. Unreacted BP and other volatile compounds are removed by thermal annealing (150°C for 30 min), which results in the partial restoration of the sp^2 bonds. The nanomaterial:BP ratio used in this study was 1:0.5 to fabricate scaffolds with >80% porosity. Chemical characterization of CNT scaffolds was performed using Raman spectroscopy and high-resolution X-ray photoelectron spectroscopy (XPS). These results showed that the primary composition of the scaffolds was carbon (~94%) and oxygen (~5.5%). It was also confirmed that radical initiated cross-linking of CNTs leads to the structural disruption of pristine nanotubes and the presence of hydroxyl, phenyl, and carbonyl and benzoyloxyl functional groups was observed. The thermal annealing step removes these oxidative functional groups and other volatiles and reaction by-products formed during the cross-linking reaction.

The presence of nanoscale cross-links between individual and bundled CNTs was confirmed using SEM and high-resolution TEM.[40] SEM imaging was performed to characterize the scaffold topography and pore architecture and reconfirm the presence of cross-links between MWCNTs and SWCNTs. Figure 1(C) (yellow arrows) confirms the presence of nanoscale cross-links between individual and bundled MWCNTs and SWCNTs. Irregularly shaped macro, micro, and nano pores are clearly visible. PLGA scaffolds show characteristic cubic shaped pores due to salt leaching of NaCl crystals [Fig. 1(C)]. MicroCT was performed to characterize the pore sizes and porosity of PLGA, MWCNT, and SWCNT scaffolds. MicroCT has been extensively used for the characterization of the porosity of 3-D all-carbon and polymeric tissue engineering scaffolds.[40,52,53] Representative microCT reconstructions of 3-D PLGA, MWCNT, and SWCNT scaffolds are shown in Figure 1(D). MicroCT images clearly show the presence of irregularly shaped interconnected pores (blue voids) distributed throughout MWCNT and SWCNT scaffolds. The white solid structures in the microCT images possess nanoscale pores that are not visualized due to the resolution limit (6 µm) of the system. These pores are characterized using SEM image processing. For diffusion and mass transport of nutrients and waste metabolites and multifold stem cell expansion, 3-D scaffolds with interconnected macro-, micro-, and nanoporosities are desired. MicroCT and SEM image processing clearly shows that 3-D MWCNT and SWCNT scaffolds possess multiscale interconnected porosities.

LDH assay was performed to quantitatively measure the cytotoxicity of MWCNT and SWCNT scaffolds against ADSCs after 1, 3, and 5 days of culture. Porous PLGA scaffolds were used as live controls. LDH assay is a widely recommended method to analyze the cytotoxicity of carbon nanomaterials.[27,54–56] It has been extensively reported that several assays (such as MTT and XTT) produce erroneous results due to nonspecific binding of formazan crystals on nanotube surface.[55,57,58] LDH assay measures cell death by quantifying the amount of cytosolic enzyme lactate dehydrogenase released in the media by apoptotic and necrotic cells. Therefore, no formazan–nanotube interference is observed. LDH assay has been widely used for the cytotoxicity analysis of carbon nanomaterials.[59] We observed no significant differences in the total LDH released by ADSCs cultured on PLGA, MWCNT, and SWCNT scaffolds at all time points [Fig. 2(A)]. These results suggest that MWCNT and SWCNT

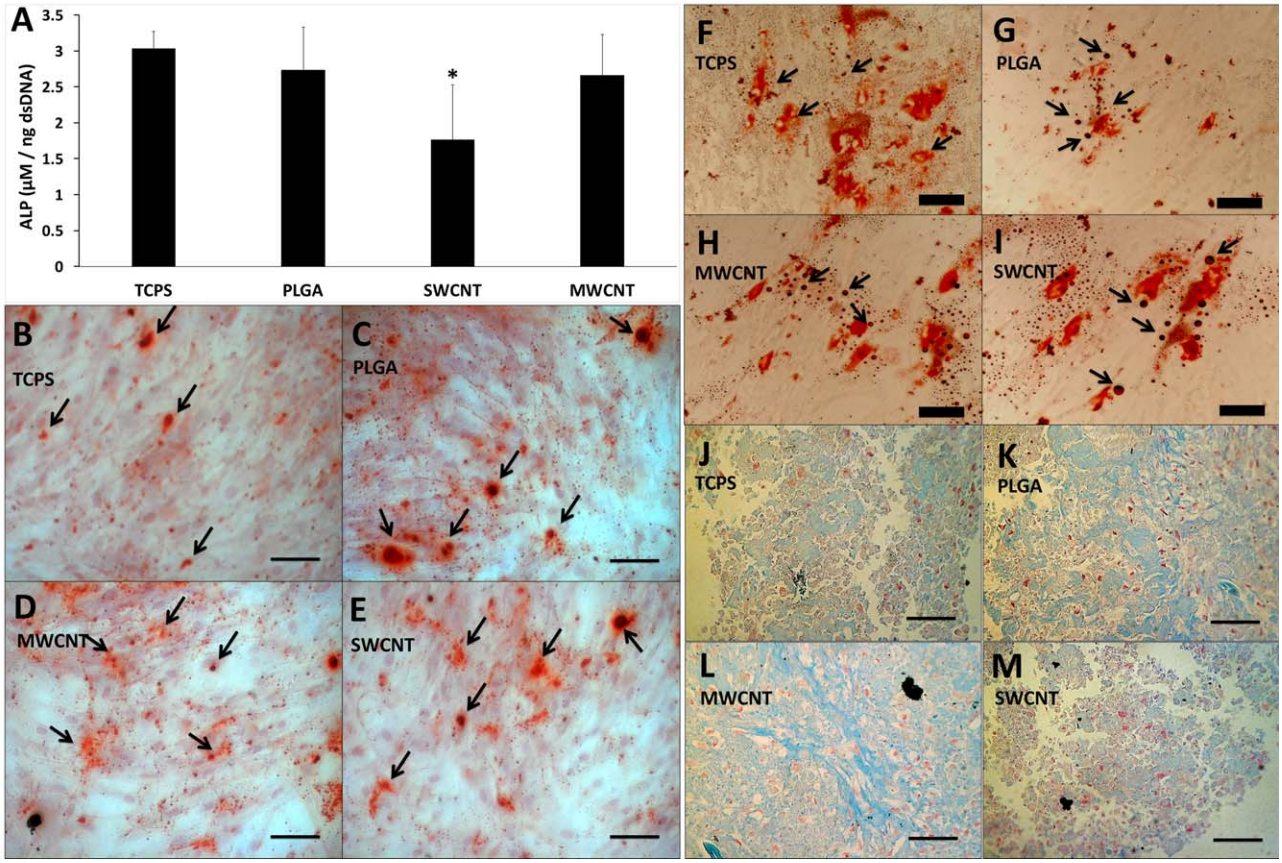

FIGURE 6. A: Alkaline phosphatase activity of ADSCs maintained on TCPS (control group) and ADSCs harvested after 30 days of expansion on PLGA, MWCNT, and SWCNT scaffolds and subsequently subjected to *in vitro* osteogenic differentiation. Data is represented as means ± standard deviation. Groups with a significant difference ($p < 0.05$) are marked with "*". (B–E) Representative alizarin red-stained images of ADSCs expanded on (B) TCPS (control), (C) PLGA, (D) MWCNT, and (E) SWCNT scaffolds. Deposits of calcium in the extracellular matrix are stained red (black arrows). Scale bars are 100 μm. (F–I) Representative oil-red O-stained images of ADSCs expanded on (F) TCPS (control), (G) PLGA, (H) MWCNT, and (I) SWCNT scaffolds. Fat vacuoles are stained red (black arrows). Scale bars are 50 μm. (J–M) Representative Alcian blue-stained images of ADSCs expanded on (J) TCPS (control), (K) PLGA, (L) MWCNT, and (M) SWCNT scaffolds. Cartilaginous extracellular matrix containing sulfated glycosaminoglycan deposits are stained blue. Scale bars are 100 μm.

scaffolds are cytocompatible, comparable to FDA-approved PLGA polymer. To further corroborate the results of LDH assay, ADSCs after 1, 3, 5, 15, and 30 days of culture on PLGA, MWCNT, and SWCNT scaffolds were stained with calcein-AM, a fluorescent marker of metabolically active living cells.[27] Green fluorescence observed in Figure 2(B(1–15)) confirms the presence of live ADSCs on all scaffold groups at all time points. Furthermore, an increase in cell number can be observed between 1 and 30 days for all scaffold groups suggesting that ADSCs on MWCNT and SWCNT scaffolds show good cell proliferation.

In mammalian cells, vinculin protein is responsible for the formation of macromolecular assemblies such as focal adhesions that link integrin proteins to the actin cytoskeleton of cells, thereby facilitating cell attachment to the underlying ECM.[46,60] Focal adhesion complexes govern several cellular functions and modulate the expression (up/down regulation) of genes associated with cell proliferation, migration, and apoptosis.[61] Immunofluorescence imaging of ADSCs confirm the presence of vinculin protein [red fluorescence, Fig. 3(A–I)] distributed throughout the cytoplasm [green fluorescence, Fig. 3(A–I)]. These results suggest that ADSCs can form focal adhesion complexes on MWCNT and SWCNT scaffolds. Ki-67 is a cell proliferation marker, which is expressed only during the active phases of the cell cycle (G1, S, G2, and M) and absent during the resting phase (G0) and has been extensively used as a marker for cell proliferation.[47,62] ADSC cultured on MWCNT and SWCNT scaffolds express Ki-67 gene [red fluorescence, Fig. 3(J–R)]. These results suggest that ADSCs are metabolically active and can proliferate on MWCNT and SWCNT scaffolds.

Cellular infiltration into 3-D scaffolds is critical to achieve greater cell densities post stem cell expansion. It is well known that cell infiltration into 3-D scaffolds is governed by the turnover of vinculin (focal adhesion assemblies).[46] Furthermore, the expression of vinculin is diffusely distributed throughout the cytoplasm in cells growing on 3-D substrates.[63] ADSCs on MWCNT and SWCNT scaffolds express a cytoplasmic distribution of vinculin, thereby suggesting that ADSCs are capable of infiltration inside the 3-D scaffolds. For cells embedded in a 3-D matrix, filopodia or cytoplasmic extensions are responsible for governing cellular

infiltration.[46] SEM analysis (Fig. 4) of ADSCs on PLGA, MWCNT, and SWCNT scaffolds show the attachment of ADSCs and the presence of numerous cytoplasmic extensions or filopodia [Fig. 4(D,E); yellow arrows]. The spectrally color-coded images of ADSCs on MWCNT and SWCNT scaffolds [Fig. 4(F–H)] confirm cellular infiltration up to depths of ~400–450 μm in MWCNT and SWCNT scaffolds. Image acquisition beyond this depth was not possible due to limitations associated with the depth of penetration of the laser.

Mesenchymal and Tissue Stem Cell Committee of ISCT have issued the following guidelines to define human MSCs for laboratory research and preclinical investigations.[43] (1) MSCs must be plastic adherent when cultured *in vitro* on TCPS. (2) More than 95% of MSCs should express CD73 (a.k.a. ecto 5′ nucleotidase), CD90 (a.k.a. Thy-1), and CD105 (a.k.a. endoglin), and lack the expression of CD14 (marker of monocytes and macrophages), CD19 (B cell marker), CD34 (hematopoietic progenitor marker), and CD45 (pan-leukocyte marker). (3) The cells must be able to demonstrate multilineage differentiation potential by differentiating into osteoblasts, adipocytes, and chondrocytes demonstrated by alizarin red, oil red O, and Alcian blue staining, respectively. Surface antigens have been extensively used for the characterization of various cell types. Figure 5(A–U) shows the representative immunofluorescence images of various surface markers of ADSCs after 15 days of culture on PLGA, MWCNT, and SWCNT scaffolds. ADSCs on all scaffold groups satisfy the ISCT criteria for the presence of MSC surface markers.

ADSCs from PLGA, MWCNT, and SWCNT scaffolds were harvested by trypsinization and expanded *in vitro* thereby demonstrating their adherence to TCPS. The ADSCs were then subjected to multilineage differentiation. Figure 6(A) shows the ALP activity of ADSCs after 30 days of culture on various scaffold groups. ALP is an early stage marker of osteogenesis.[45] No significant differences were observed in the ALP activity of ADSCs cultured on PLGA and MWCNT scaffolds, compared to normal TCPS ADSCs (control group). Although, ADSCs cultured on SWCNT scaffolds showed a lower ALP activity, the deposition of calcium in the ECM of ADSCs of all scaffold groups observed by alizarin red staining [Fig. 6(B–E)] confirms their successful osteogenic differentiation. Oil red O staining shows the presence of lipid vacuoles [Fig. 6(F–I)], black arrows) in ADSCs of all scaffold groups thereby confirming their adipogenic differentiation. Alcian blue staining [Fig. 6(J–M)] shows the presence of cartilaginous ECM (deposition of sulfated GAGs) by ADSCs of all scaffold groups thereby confirming their differentiation into chondrocytes. These results taken together suggest that ADSCS cultured on 3-D MWCNT and SWCNT scaffolds satisfy all the criteria that define human MSCs as recommended by ISCT. Therefore, 3-D MWCNT and SWCNT scaffolds can be used as novel synthetic matrices for stem cell expansion and maintenance.

Bone marrow (BM) aspirates are the most commonly used source for the isolation of MSCs (BMSCs). However, the prevalence of adult MSCs in BM aspirates is very low (approximately 0.0001–0.01%).[64] Furthermore, the number of MSCs drastically reduces from BM aspirates of elderly due to aging.[65] A convenient alternative is to isolate MSCs from adipose tissue, which can be obtained by a simple liposuction procedure in clinic. The number of MSCs isolated from adipose tissue is nearly 500-fold greater compared to an equivalent amount of BM aspirate.[66,67] It has been shown that ADSCs and BMSCs exhibit similar multilineage differentiation potential and immunosuppressive properties with minor differences in transcriptome and proteome. Human ADSCs are genetically stable in long-term cell culture, show a higher proliferation capacity and rate (doubling time for ADSCs is 28 h, whereas 39 h for BMSCs), and retain multilineage differentiation potential for longer time periods compared to BMSCs.[65,68–70] Owing to these advantages, stem cells derived from adipose tissue are an attractive alternative to bone marrow-derived stem cells for clinical tissue engineering and regenerative medicine applications.

Stem cell therapy for conditions such as bone and cartilage defects, graft vs. host disease, myocardial infarction, and autoimmune diseases requires ~4–5 million cells per kg body weight.[3,7,71] It is difficult to isolate MSCs in clinically relevant number from diseased patients or elderly donors who typically are the patients in need of therapy. Currently, the large-scale expansion of MSCs for therapy is an unmet clinical need as the cells undergo significant changes in phenotype such as diminished proliferation potential, senescence, or loss of "stemness" (onset of lineage specific phenotypic characteristics) during prolonged culture on TCPS substrates. Consequently, to achieve high cell densities and maintain a greater pool of stem cells, 3-D culture systems have been recommended for MSC expansion over conventional 2-D substrates.[3,6,7] The 3-D cross-linked CNT scaffolds may allow additional multifunctional capabilities compared to existing 3-D culture systems such as cell aggregates, use of microcarriers, polymeric matrices, or decellularized matrices. (1) The mechanical (nanotopography and stiffness), electromagnetic, and electrical properties of CNT scaffolds and ability to covalently or noncovalently functionalize them with a variety of small molecules or macromolecules can be exploited as a biophysical cue to control the spatiotemporal behavior of stem cells.[72,73] (2) CNTs have been reported as contrast agents for several noninvasive bioimaging modalities such as magnetic resonance imaging, photoacoustic, and X-ray computed tomography.[74–76] Thus, 3-D CNT scaffolds may facilitate noninvasive longitudinal monitoring of stem cell maintenance, proliferation, and differentiation.

CONCLUSIONS

Three-dimensional macroporous scaffolds fabricated using SWCNTs and MWCNTs are cytocompatible substrates that show good cell viability, adhesion, proliferation, and infiltration of human ADSCs. ADSCs after long-term expansion on MWCNT and SWCNT scaffolds retain their stem cell phenotype (express MSC surface antigens), can be harvested from 3-D MWCNT and SWCNT scaffolds, and show robust multilineage differentiation into osteoblasts, adipocytes, and chondrocytes. These results indicate that 3-D macroporous MWCNT and SWCNT scaffolds show potential as synthetic

3-D matrices for *ex vivo* expansion and maintenance of MSCs for clinical therapeutic applications.

ACKNOWLEDGMENT

The authors thank Dr Stefan Judex and Dr Jeyantt Sankaran for the help with microCT data acquisition. This work was supported by the the National Institutes of Health (grants No. 1DP2OD007394-01).

REFERENCES

1. Uccelli A, Moretta L, Pistoia V. *Mesenchymal stem cells in health and disease*. Nat Rev Immunol 2008; 8: 726–736.
2. Madrigal M, Rao KS, Riordan NH. *A review of therapeutic effects of mesenchymal stem cell secretions and induction of secretory modification by different culture methods*. J Transl Med 2014; 12: 260.
3. Ng CP, Sharif ARM, Heath DE, Chow JW, Zhang CB, Chan-Park MB, Hammond PT, Chan JK, Griffith LG. *Enhanced ex vivo expansion of adult mesenchymal stem cells by fetal mesenchymal stem cell ECM*. Biomaterials 2014; 35: 4046–4057.
4. Vacanti V, Kong E, Suzuki G, Sato K, Canty JM, Lee T. *Phenotypic changes of adult porcine mesenchymal stem cells induced by prolonged passaging in culture*. J Cell Physiol 2005; 205: 194–201.
5. Javazon EH, Beggs KJ, Flake AW. *Mesenchymal stem cells: Paradoxes of passaging*. Exp Hematol 2004; 32: 414–425.
6. Chase LG, Lakshmipathy U, Solchaga LA, Rao MS, Vemuri MC. *A novel serum-free medium for the expansion of human mesenchymal stem cells*. Stem Cell Res Therap 2010; 1: 8.
7. Jung S, Panchalingam KM, Rosenberg L, Behie LA. *Ex vivo expansion of human mesenchymal stem cells in defined serum-free media*. Stem Cell Int 2012;2012:
8. Meng X, Leslie P, Zhang Y, Dong J. *Stem cells in a three-dimensional scaffold environment*. Springerplus 2014; 3:80.
9. Singh H, Mok P, Balakrishnan T, Rahmat SNB, Zweigerdt R. *Up-scaling single cell-inoculated suspension culture of human embryonic stem cells*. Stem Cell Res 2010; 4: 165–179.
10. Amit M, Laevsky I, Miropolsky Y, Shariki K, Peri M, Itskovitz-Eldor J. *Dynamic suspension culture for scalable expansion of undifferentiated human pluripotent stem cells*. Nat Protocols 2011; 6: 572–579.
11. SerraBrito MC, Alves PM. *Bioengineering strategies for stem cell expansion and differentiation*. Canal Bioquímica 2010; 7:30–38.
12. Jing D, Parikh A, Tzanakakis ES. *Cardiac cell generation from encapsulated embryonic stem cells in static and scalable culture systems*. Cell Transplant 2010; 19: 1397.
13. Storm MP, Orchard CB, Bone HK, Chaudhuri JB, Welham MJ. *Three-dimensional culture systems for the expansion of pluripotent embryonic stem cells*. Biotechnol Bioeng 2010;107:683–695.
14. Serra M, Correia C, Malpique R, Brito C, Jensen J, Bjorquist P, Carrondo MJ, Alves PM. *Microencapsulation technology: A powerful tool for integrating expansion and cryopreservation of human embryonic stem cells*. PLoS One 2011; 6: e23212.
15. Leist CH, Meyer H-P, Fiechter A. *Potential and problems of animal cells in suspension culture*. J Biotechnol 1990; 15: 1–46.
16. Malda J, Frondoza CG. *Microcarriers in the engineering of cartilage and bone*. Trends Biotechnol 2006; 24: 299–304.
17. Lei Y, Schaffer DV. *A fully defined and scalable 3D culture system for human pluripotent stem cell expansion and differentiation*. Proc Natl Acad Sci 2013; 110: E5039–E5048.
18. Braccini A, D, Wendt C, Jaquiery M, Jakob M, Heberer L, Kenins A, Wodnar-Filipowicz R, Quarto I. Martin *Three-dimensional perfusion culture of human bone marrow cells and generation of osteoinductive grafts*. Stem Cells 2005;23:1066–1072.
19. Papadimitropoulos A, Piccinini E, Brachat S, Braccini A, Wendt D, Barbero A, Jacobi C, Martin I. *Expansion of human mesenchymal stromal cells from fresh bone marrow in a 3D scaffold-based system under direct perfusion*. PLoS One 2014; 9: e102359.
20. Chen XD, Dusevich V, Feng JQ, Manolagas SC, Jilka RL. *Extracellular matrix made by bone marrow cells facilitates expansion of marrow-derived mesenchymal progenitor cells and prevents their differentiation into osteoblasts*. J Bone Miner Res 2007;22:1943–1956.
21. Volkmer E, Drosse I, Otto S, Stangelmayer A, Stengele M, Kallukalam BC, Mutschler W, Schieker M. *Hypoxia in static and dynamic 3D culture systems for tissue engineering of bone*. Tissue Eng A 2008; 14: 1331–1340.
22. Grayson WL, Zhao F, Izadpanah R, Bunnell B, Ma T. *Effects of hypoxia on human mesenchymal stem cell expansion and plasticity in 3D constructs*. J Cell Physiol 2006; 207: 331–339.
23. Lalwani G, Sitharaman B. *Multifunctional fullerene- and metallofullerene-based nanobiomaterials*. Nano LIFE 2013; 3: 1342003-1-22.
24. Lalwani G, Henslee AM, Farshid B, Parmar P, Lin L, Qin Y-X, Kasper FK, Mikos AG, Sitharaman B. *Tungsten disulfide nanotubes reinforced biodegradable polymers for bone tissue engineering*. Acta Biomater 2013; 9: 8365–8373.
25. Lalwani G, Henslee AM, Farshid B, Lin L, Kasper FK, Qin Y-X, Mikos AG, Sitharaman B. *Two-dimensional nanostructure-reinforced biodegradable polymeric nanocomposites for bone tissue engineering*. Biomacromolecules 2013; 14: 900–909.
26. Lalwani G, Cai X, Nie L, Wang LV, Sitharaman B. *Graphene-based contrast agents for photoacoustic and thermoacoustic tomography*. Photoacoustics 2013; 1: 62–67.
27. Lalwani G, Sundararaj JL, Schaefer K, Button T, Sitharaman B. *Synthesis, characterization, in vitro phantom imaging, and cytotoxicity of a novel graphene-based multimodal magnetic resonance imaging-X-ray computed tomography contrast agent*. J Mater Chem B 2014; 2: 3519–3530.
28. Kanakia S, Toussaint JD, Chowdhury S, Lalwani M, Tembulkar G, Button TT, Shroyer K, Moore RW, Sitharaman B. *Physicochemical characterization of a novel graphene-based magnetic resonance imaging contrast agent*. Int J Nanomed 2013; 8:2821–2833.
29. Lalwani G, D'agati M, Khan AM, Sitharaman B. *Toxicology of graphene-based nanomaterials*. Adv Drug Deliv Rev 2016; 105: 109–144.
30. Patel SC, Lee S, Lalwani G, Suhrland C, Chowdhury SM, Sitharaman B. *Graphene-based platforms for cancer therapeutics*. Therap Deliv 2016; 7: 101–116.
31. Xing W, Lalwani G, Rusakova I, Sitharaman B. *Degradation of graphene by hydrogen peroxide*. Part Part Syst Charact 2014; 31: 745–750.
32. Harrison BS, Atala A. *Carbon nanotube applications for tissue engineering*. Biomaterials 2007; 28: 344–353.
33. Brunner EW, Jurewicz I, Heister E, Fahimi A, Bo C, Sear RP, Donovan PJ, Dalton AB. *Growth and proliferation of human embryonic stem cells on fully synthetic scaffolds based on carbon nanotubes*. ACS Appl Mater Interface 2014; 6: 2598–2603.
34. Holy J, Perkins E, Yu X. *Differentiation of pluripotent stem cells on multiwalled carbon nanotubes*. In: *Engineering in Medicine and Biology Society, 2009. EMBC 2009. Annual International Conference of the IEEE*. 2009. IEEE.
35. Martinelli V, Cellot G, Toma FM, Long CS, Caldwell JH, Zentilin L, Giacca M, Turco A, Prato M, Ballerini L. *Carbon nanotubes promote growth and spontaneous electrical activity in cultured cardiac myocytes*. Nano Lett 2012; 12: 1831–1838.
36. Pryzhkova MV, Aria I, Cheng Q, Harris GM, Zan X, Gharib M, Jabbarzadeh E. *Carbon nanotube-based substrates for modulation of human pluripotent stem cell fate*. Biomaterials 2014; 35: 5098–5109.
37. Mooney E, Dockery P, Greiser U, Murphy M, Barron V. *Carbon nanotubes and mesenchymal stem cells: Biocompatibility, proliferation and differentiation*. Nano Lett 2008; 8: 2137–2143.
38. Correa-Duarte MA, Wagner N, Rojas-Chapana J, Morsczeck C, Thie M, Giersig M. *Fabrication and biocompatibility of carbon nanotube-based 3D networks as scaffolds for cell seeding and growth*. Nano Lett 2004; 4: 2233–2236.
39. Abarrategi A, Gutiérrez MC, Moreno-Vicente C, Hortigüela MJ, Ramos V, López-Lacomba JL, Ferrer ML, del Monte F. *Multiwall carbon nanotube scaffolds for tissue engineering purposes*. Biomaterials 2008; 29: 94–102.
40. Lalwani G, Kwaczala AT, Kanakia S, Patel SC, Judex S, Sitharaman B. *Fabrication and characterization of three-dimensional macroscopic all-carbon scaffolds*. Carbon 2013;53:90–100.
41. Lalwani G, Gopalan A, D'Agati M, Srinivas Sankaran J, Judex S, Qin YX, Sitharaman B. *Porous three-dimensional carbon*

nanotube scaffolds for tissue engineering. J Biomed Mater Res A 2015;103:3212–3225.
42. Patel SC, Lalwani G, Grover K, Qin Y-X, Sitharaman B. *Fabrication and cytocompatibility of in situ crosslinked carbon nanomaterial films*. Sci Rep 2015; 5:
43. Dominici M, Le Blanc K, Mueller I, Slaper-Cortenbach I, Marini F, Krause D, Deans R, Keating A, Prockop D, Horwitz E. *Minimal criteria for defining multipotent mesenchymal stromal cells. The International Society for Cellular Therapy position statement*. Cytotherapy 2006; 8: 315–317.
44. Cai X, Paratala BS, Hu S, Sitharaman B, Wang LV. *Multiscale photoacoustic microscopy of single-walled carbon nanotube-incorporated tissue engineering scaffolds*. Tissue Eng C Met 2011; 18: 310–317.
45. Talukdar Y, Rashkow JT, Lalwani G, Kanakia S, Sitharaman B. *The effects of graphene nanostructures on mesenchymal stem cells*. Biomaterials 2014; 35: 4863–4877.
46. Fraley SI, Feng Y, Krishnamurthy R, Kim D-H, Celedon A, Longmore GD, Wirtz D. *A distinctive role for focal adhesion proteins in three-dimensional cell motility*. Nat Cell Biol 2010; 12: 598–604.
47. Scholzen T, Gerdes J. *The Ki-67 protein: From the known and the unknown*. J Cell Physiol 2000;182:311–322.
48. Granéli C, Thorfve A, Ruetschi U, Brisby H, Thomsen P, Lindahl A, Karlsson C. *Novel markers of osteogenic and adipogenic differentiation of human bone marrow stromal cells identified using a quantitative proteomics approach*. Stem Cell Res 2014; 12: 153–165.
49. Mehlem A, Hagberg CE, Muhl L, Eriksson U, Falkevall A. *Imaging of neutral lipids by oil red O for analyzing the metabolic status in health and disease*. Nat Protocols 2013; 8: 1149–1154.
50. Ullah M, Hamouda H, Stich S, Sittinger M, Ringe J. *A reliable protocol for the isolation of viable, chondrogenically differentiated human mesenchymal stem cells from high-density pellet cultures*. BioRes Open Access 2012; 1: 297–305.
51. Lalwani G, D'agati M, Gopalan A, Rao M, Schneller J, Sitharaman B. *Three-dimensional macroporous graphene scaffolds for tissue engineering*. J Biomed Mater Res A 2017;105:73–83.
52. Guarino V, Guaccio A, Netti PA, Ambrosio L. *Image processing and fractal box counting: User-assisted method for multi-scale porous scaffold characterization*. J Mater Sci Mater Med 2010; 21: 3109–3118.
53. McCullen SD, Stevens DR, Roberts WA, Clarke LI, Bernacki SH, Gorga RE, Loboa EG. *Characterization of electrospun nanocomposite scaffolds and biocompatibility with adipose-derived human mesenchymal stem cells*. Int J Nanomed 2007; 2: 253.
54. Chowdhury SM, Lalwani G, Zhang K, Yang JY, Neville K, Sitharaman B. *Cell specific cytotoxicity and uptake of graphene nanoribbons*. Biomaterials 2013; 34: 283–293.
55. Wörle-Knirsch J, Pulskamp K, Krug H. *Oops they did it again! Carbon nanotubes hoax scientists in viability assays*. Nano Lett 2006; 6: 1261–1268.
56. Avti PK, Caparelli ED, Sitharaman B. *Cytotoxicity, cytocompatibility, cell-labeling efficiency, and in vitro cellular magnetic resonance imaging of gadolinium-catalyzed single-walled carbon nanotubes*. J Biomed Mater Res A 2013;101:3580–3591.
57. Belyanskaya L, Manser P, Spohn P, Bruinink A, Wick P. *The reliability and limits of the MTT reduction assay for carbon nanotubes–cell interaction*. Carbon 2007; 45: 2643–2648.
58. Casey A, Herzog E, Davoren M, Lyng F, Byrne H, Chambers G. *Spectroscopic analysis confirms the interactions between single walled carbon nanotubes and various dyes commonly used to assess cytotoxicity*. Carbon 2007; 45: 1425–1432.
59. Farshid B, Lalwani G, Sitharaman B. *In vitro cytocompatibility of one-dimensional and two-dimensional nanostructure-reinforced biodegradable polymeric nanocomposites*. J Biomed Mater Res A 2015;103:2309–2321.
60. DeMali KA. *Vinculin–a dynamic regulator of cell adhesion*. Trends Biochem Sci 2004; 29: 565–567.
61. Livshits G, Kobielak A, Fuchs E. *Governing epidermal homeostasis by coupling cell–cell adhesion to integrin and growth factor signaling, proliferation, and apoptosis*. Proc Natl Acad Sci 2012; 109: 4886–4891.
62. Schlüter C, Duchrow M, Wohlenberg C, Becker M, Key G, Flad H-D, Gerdes J. *The cell proliferation-associated antigen of antibody Ki-67: A very large, ubiquitous nuclear protein with numerous repeated elements, representing a new kind of cell cycle-maintaining proteins*. J Cell Biol 1993; 123: 513–522.
63. Mierke CT, Kollmannsberger P, Zitterbart DP, Diez G, Koch TM, Marg S, Ziegler WH, Goldmann WH, Fabry B. *Vinculin facilitates cell invasion into three-dimensional collagen matrices*. J Biol Chem 2010; 285: 13121–13130.
64. Ester Bernardo M, Locatelli F, FIBBE WE. *Mesenchymal stromal cells: A novel treatment modality for tissue repair*. Ann N Y Acad Sci 2009; 1176:101–117.
65. Puissant B, Barreau C, Bourin P, Clavel C, Corre J, Bousquet C, Taureau C, Cousin B, Abbal M, Laharrague P. *Immunomodulatory effect of human adipose tissue-derived adult stem cells: Comparison with bone marrow mesenchymal stem cells*. Br J Haematol 2005;129:118–129.
66. Hass R, Kasper C, Böhm S, Jacobs R. *Different populations and sources of human mesenchymal stem cells (MSC): A comparison of adult and neonatal tissue-derived MSC*. Cell Commun Signal 2011; 9: 1.
67. Fraser JK, Wulur I, Alfonso Z, Hedrick MH. *Fat tissue: An underappreciated source of stem cells for biotechnology*. Trends Biotechnol 2006; 24: 150–154.
68. Yoo KH, Jang IK, Lee MW, Kim HE, Yang MS, Eom Y, Lee JE, Kim YJ, Yang SK, Jung HL. *Comparison of immunomodulatory properties of mesenchymal stem cells derived from adult human tissues*. Cell Immunol 2009; 259: 150–156.
69. Zhu X, Du J, Liu G. *The comparison of multilineage differentiation of bone marrow and adipose-derived mesenchymal stem cells*. Clin Lab 2011; 58: 897–903.
70. Strioga M, Viswanathan S, Darinskas A, Slaby O, Michalek J. *Same or not the same? Comparison of adipose tissue-derived versus bone marrow-derived mesenchymal stem and stromal cells*. Stem Cell Dev 2012; 21: 2724–2752.
71. Binato R, T, de Souza Fernandez C, Lazzarotto-Silva B, Du Rocher A, Mencalha L, Pizzatti L, Bouzas E. Abdelhay *Stability of human mesenchymal stem cells during in vitro culture: Considerations for cell therapy*. Cell Prolif 2013; 46: 10–22.
72. Bianco A, Kostarelos K, Prato M. *Applications of carbon nanotubes in drug delivery*. Curr Opin Chem Biol 2005; 9: 674–679.
73. Lalwani G, Patel SC, Sitharaman B. *Two- and three-dimensional all-carbon nanomaterial assemblies for tissue engineering and regenerative medicine*. Ann Biomed Eng 2016; 1–16.
74. Sitharaman B, Kissell KR, Hartman KB, Tran L, Baikalov A, Rusakova A, Sun IY, Khant HA, Ludtke SJ, Chiu W. *Superparamagnetic gadonanotubes are high-performance MRI contrast agents*. Chem Commun 2005; 3915–3917.
75. Pramanik M, Swierczewska M, Green D, Sitharaman B, Wang LV. *Single-walled carbon nanotubes as a multimodal-thermoacoustic and photoacoustic-contrast agent*. J Biomed Opt 2009; 14: 034018-034018-8.
76. Rivera EJ, Tran LA, Hernández-Rivera M, Yoon D, Mikos AG, Rusakova IA, Cheong BY, da Graça Cabreira-Hansen M, Willerson JT, Perin EC. *Bismuth@ US-tubes as a potential contrast agent for X-ray imaging applications*. J Mater Chem B 2013; 1: 4792–4800.